



Analyzing the early structural build-up of accelerated cement pastes

Tobias Dorn · Tamino Hirsch · Dietmar Stephan

Received: 28 July 2020 / Accepted: 14 February 2021 / Published online: 10 March 2021
© The Author(s) 2021

Abstract Extrusion-based additive manufacturing imposes high requirements on the material stability right after the extrusion. Therefore, a thorough understanding of the chemical reactions that determine the early reduction in processability is necessary. Accelerators are especially considered here, which have a major influence on the early reaction. This study contributes to these issues by analyzing the influence of 0.1 wt% TEA (triethanolamine) and 2.0 wt% $\text{Ca}(\text{NO}_3)_2$ on the hydration of two CEM I 52.5 R. The hydration was analyzed by isothermal heat flow calorimetry and in-situ X-ray diffraction. Vicat needle penetration, a penetrometer of own design, and ultrasonic P-wave velocity development were used to monitor the early change in workability. The obtained results indicate that ettringite formation is the main factor influencing workability during the first 60 min of hydration. Afterwards, the influence of ettringite is exceeded by the formation of C–S–H. $\text{Ca}(\text{NO}_3)_2$ was shown to enhance C–S–H formation and had no significant effect on the workability during the first 60 min of hydration while rapidly decreasing workability during the induction period. TEA was shown to increase brownmillerite dissolution and

ettringite formation and, consequently, promote the workability loss during the initial hydration period. The time of initial and final setting determined by the Vicat needle test depended mainly on the formation of C–S–H phases.

Keywords Cement hydration · Acceleration · Calcium nitrate · Triethanolamine · OPC · In-situ X-ray diffraction

1 Introduction

Digital fabrication describes the combination of computer-aided design (CAD) and automated additive as well as subtractive manufacturing technologies. As the additive manufacturing of large-scale components using concrete or mortar extrusion has several advantages over conventional concreting, it has been gaining increasing attention in research and industry [1, 2]. The most important advantages of this newly developed technology are the high freedom of design achievable as well as the time and cost savings from the elimination of formwork in this process [3]. Without formwork, however, the requirements imposed on the material are significantly higher, as all the requirements usually fulfilled by the formwork must now be fulfilled by the material itself [3, 4]. Lim et al. [5] define the main characteristics of

T. Dorn (✉) · T. Hirsch · D. Stephan
Institute of Civil Engineering, Group of Building
Materials and Construction Chemistry, Technische
Universität Berlin, Gustav-Meyer-Allee 25, 13355 Berlin,
Germany
e-mail: t.dorn@tu-berlin.de



printable mortars. Among other material characteristics, they describe the “printability” as the ease and reliability of material deposition and the “buildability” as the resistance of deposited wet material to deformation under load. Perrot et al. [6] conclude that the printability and the buildability of material are competing factors that need to be optimized in order to achieve additively manufactured large-scale components. However, this optimization requires a thorough understanding of early cement hydration and the chemical reactions controlling workability reduction. Cement accelerators, introduced into the material just before extrusion, might be a reliable option for materials to combine high printability with a high buildability in additive manufacturing.

Conventionally the effect of accelerators on the workability of cement pastes is expressed as the reduction of setting time determined by the Vicat needle penetration test depending on the accelerator concentration. The fact that an accelerated cement paste might significantly change its workability before the initial setting time is widely ignored. However, to produce mortars with an optimized printability and buildability, a thorough understanding of the early workability change of accelerated cementitious materials is required.

The present study analyzes the continuous change in the workability of two CEM I 52.5 R accelerated with 2.0 wt% $\text{Ca}(\text{NO}_3)_2$ and 0.1 wt% TEA (triethanolamine) respectively, using a penetrometer of our own design and by measuring the development of ultrasonic P-wave velocity (v_p). The initial and final setting times, according to EN 196-3 [7], were also recorded. In order to get an understanding of the hydration processes leading to the observed change in workability in the analyzed samples, isothermal calorimetry and in-situ X-ray diffraction (XRD) were applied. A correlation between the hydration product formation and the workability reduction was drawn to identify the processes most relevant to the workability reduction at different times during the early hydration of accelerated cement pastes.

2 Theoretical framework

There is a general agreement in the literature that the early hydration and thus the early change in workability of hydrating cement pastes is mainly due to two

chemical reactions. These are the reaction of tricalcium aluminate, calcium sulfate, and water to predominate ettringite and the reaction of alite and water to C–S–H and portlandite [8, 9].

In-situ XRD in combination with isothermal heat flow calorimetry can be effectively used to understand the dissolution and crystallization processes within hydrating cement pastes [10–15]. Results presented by Jansen et al. [12] reveal that the initial heat flow measured in calorimetry originates from the partial dissolution of tricalcium aluminate, the complete dissolution of sulfate-containing clinker phases, and the initial formation of ettringite. Evidence that this initial ettringite formation is the main influence causing an early reduction in workability has been presented by Jakob et al. [14, 15], who used in-situ XRD and isothermal heat flow calorimetry in combination with rheological measurements.

The initial hydration is followed by the induction period, a period of low chemical activity during which slow C–S–H nucleation [16–19] and slow ettringite precipitation [11, 20] occur. The acceleration period, which usually sets in between 2 and 3 h of hydration for an unaccelerated cement, is dominated by the fast dissolution of alite as well as the precipitation of C–S–H and portlandite [9, 12]. It is well known that the interparticle coalescence of C–S–H phases is mainly responsible for the setting of and increase in the compressive strength of cementitious materials [21, 22]. However, the time at which the impact of the interparticle coalescence of C–S–H phases overrides the early effects of ettringite precipitation on the workability of a cement paste is still under debate [15, 23].

Accelerating admixtures significantly influence the described reactions of cement hydration and might thus alter the early ettringite precipitation, the C–S–H formation, and consequently the way in which ettringite and C–S–H influence the workability of a hydrating cementitious material.

Justness & Nygaard [24] describe two mechanisms by which $\text{Ca}(\text{NO}_3)_2$, a frequently used component of commercial accelerators and antifreeze admixtures [25], affects the cement hydration, including a faster supersaturation of pore solution in $\text{Ca}(\text{OH})_2$ and subsequent crystallization of portlandite and, due to the high calcium concentration, a depression of sulphate solubility. The efficiency of $\text{Ca}(\text{NO}_3)_2$ as a setting accelerator was proposed to depend on the



clinker composition, as some authors found it to increase with the belite content [24, 26].

TEA, conventionally used as a grinding aid for cement clinker as well as an accelerator to compensate for the retarding effect of some superplasticizers [25], might also be used as a setting accelerator in additive manufacturing [27]. The effect of TEA on the hydration of ordinary Portland cement-based materials has been discussed by [27–34]. While the precise mechanism is still under debate, there is a general agreement that TEA accelerates the hydration of the aluminate-containing phases tricalcium aluminate (C_3A) and brownmillerite (C_4AF) and consequently reduces the initial setting time while delaying the hydration of alite [27, 29, 33, 34].

As discussed above, there is a general understanding of the workability loss of Portland cement-based materials and the mechanisms by which $Ca(NO_3)_2$ and TEA accelerate cement hydration. However, more research is required, regarding the time-dependent contribution of the accelerated silicate and aluminate phase reactions on the workability loss of hydrating cement pastes, to develop cement-based materials applied in challenging applications, as 3D printing.

3 Experimental setup

3.1 Materials

Two CEM I 52.5 R [35], produced by different manufacturers and referred to as CEM A and CEM B, have been used in this study. Their chemical composition, determined by XRF, is given in Table 1. The phase content was quantified by XRD combined with Rietveld refinement (Table 2). The specific surface areas of the two cements were determined by the Blaine method, and the particle size distributions of the cements were measured using a Malvern Panalytical Mastersizer 2000 and are presented in Fig. 1. CEM A and CEM B have comparable chemical and phase compositions. However, CEM A contains besides bassanite and anhydrite also gypsum as a sulfate carrier, which was not the case for CEM B. The specific surface areas of CEM A and CEM B were $4700 \pm 100 \text{ cm}^2/\text{g}$ and $4900 \pm 100 \text{ cm}^2/\text{g}$, respectively. The particle size distribution is slightly broader for CEM B as compared to CEM A.

3.2 Mix proportions, methods, and procedure

Table 3 shows the mix proportions of the analyzed cement pastes. Samples for the Vicat needle penetration, ultrasonic P-wave velocity measurement, and the MIL-device penetration were prepared according to EN 196-3 [7]. For the calorimetric and in-situ XRD measurements, where smaller amounts of cement paste were needed, the ratios of the mix proportions were kept constant. For these smaller samples, mixing was performed using a vortex mixer at the highest level for 2 min. In each case, the accelerators were added to the cement together with the mixing water in which they were dissolved at least 24 h before the experiment. $Ca(NO_3)_2$ was added at a dosage 2 wt% and TEA at a dosage of 0.1 wt% by weight of cement. For all experiments, deionized water was used. All experiments were conducted with the water-to-cement ratio (w/c) at which the respective cement reached standard stiffness according to EN 196-3 [7].

3.3 Laser diffraction analysis

Before the measurement was started, ultrasound was applied to the cement-isopropanol suspensions for 2 min to disperse possible agglomerates. The results presented in Fig. 1 are the average of three measurements.

3.4 Vicat needle penetration

The setting time of all samples was determined according to EN 196-3 [7] using the automatic Vicat needle device ToniSET Compact. The standard stiffness of CEM A was achieved at a w/c of 0.328 and that of CEM B at a w/c ratio of 0.330. The results presented in Fig. 2 are the average of three measurements.

3.5 Ultrasonic P-wave velocity (v_p) measurement

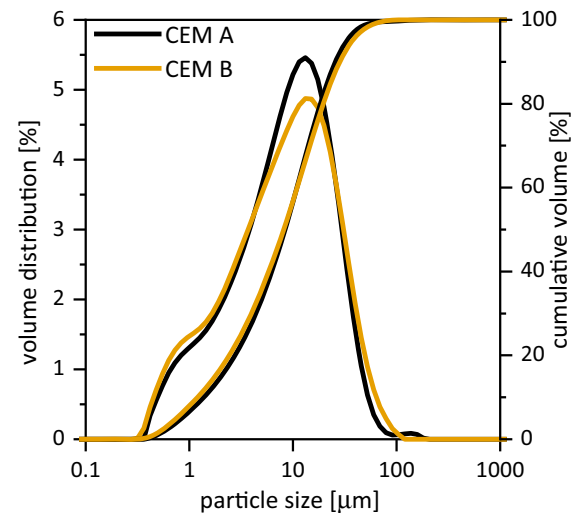
The measurement of the ultrasonic P-wave velocity was performed using an Ultratest IP8. The device measures the velocity of ultrasonic P-waves transmitting through 40 mm of cement paste. A measurement of v_p was performed every 60 s for the first 6 h of cement hydration. All tests were performed in an air-conditioned laboratory at 21 °C. The results presented in Fig. 5 are the average of three measurements.

Table 1 Oxide composition of CEM A & CEM B determined by XRF in wt%

	Al ₂ O ₃	CaO	Fe ₂ O ₃	K ₂ O	MgO	MnO	Na ₂ O	P ₂ O ₅	SiO ₂	SO ₃	TiO ₂	LOI	Sum
A	4.99	63.63	3.21	1.14	1.75	0.06	0.24	0.08	19.44	3.065	0.23	2.69	100.52
B	4.37	63.32	2.81	1.02	2.26	0.04	0.38	0.32	19.57	2.98	0.23	2.76	100.06

Table 2 Mineral composition of CEM A and CEM B determined by Rietveld refinement of XRD data

Phase	ICSD code	CEM A	CEM B
Alite	81100	61	58
Belite	81096	13	15
C ₃ A (cubic)	1841	3	2
C ₃ A (orthorhombic)	100220	2	2
Brownmillerite	9197	12	11
Gypsum	27221	0.9	0
Bassanite	79529	2	2
Anhydrite	159702	5	4
Calcite	80869	2	4
Lime	52783	0	0.2
Aphthitalite	26018	0.5	0.6
Arcanite	79777	0.5	0.4

**Fig. 1** Particle size distributions of CEM A and CEM B determined by laser diffraction analysis. The small increase at > 100 µm measured for CEM A presumably originates from air bubbles within the dispersant isopropanol

3.6 Multi-purpose incremental loading device penetration test

The resistance of the cement pastes to the penetration by a 15 mm sphere was measured using a penetrometer of our own design called the Multi-purpose Incremental Loading Device (MILD), which is described in detail by Pott et al. [13]. The sphere was inserted into the sample at a speed of 1.2 µm/s, and the required force was continuously measured. Before the measurement with the MIL-device, the sample was placed in a round plastic container with a diameter of 6 cm and a height of 8 cm. The measurement was started, with the sphere submerged in the cement paste, 5 min after the initial mixing. The MIL-device can measure a maximum force of 100 N. The presented results are the average of three measurements.

3.7 Isothermal heat flow calorimetry

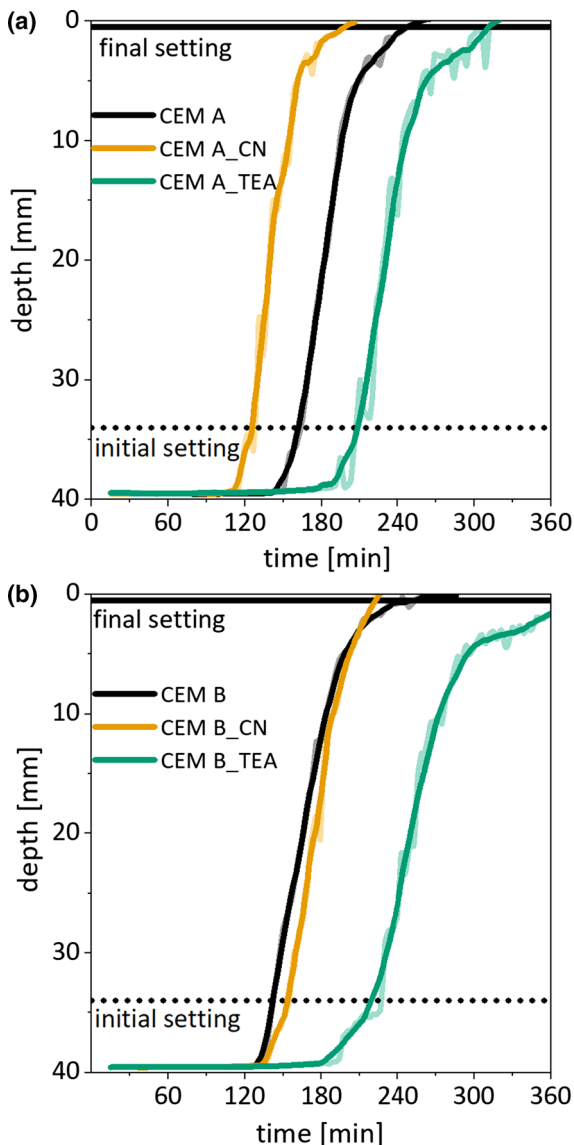
The heat flow of each sample was measured using the isothermal heat flow calorimeter MC-Cal 100P (C3 Prozess- und Analysetechnik, Germany) at a temperature of 20 °C. The results were used to calculate the cumulative heat of hydration. For each sample of CEM A, 22.07 g of cement and 7.24 g of water were used, and for each sample of CEM B, 21.98 g of cement and 7.26 g of water were used. After mixing, the samples were immediately put into the device. The heat flow was recorded every 60 s for 12 h. The presented results are normalized per g of cement and are the average of three measurements.

3.8 In-situ X-ray diffraction (XRD)

The in-situ XRD measurements were performed on a PANalytical Empyrean in Bragg–Brentano geometry using CuK_α radiation. For the measurement, approx. 5 g of cement paste was placed in a temperature-controlled sample stage set to 20 °C and covered with

Table 3 Mix proportions for samples examined

Sample	Water (g)	Cement (g)	Ca(NO ₃) ₂ (g)	TEA (g)
CEM A	164	500		
CEM A_CN	164	500	10	
CEM A_TEA	164	500		0.5
CEM B	165	500		
CEM B_CN	165	500	10	
CEM B_TEA	165	500		0.5

**Fig. 2** Smoothed results of the Vicat needle penetration, according to EN 196-3 [7]. Measured results in the background: **a** results of CEM A, **b** results of CEM B

a 7.5 μm thick Kapton® film to protect the sample against the evaporation of water and atmospheric CO₂. For evaluation, reflex intensities after background subtraction were used.

4 Results

4.1 Vicat needle penetration

Figure 2 presents the results of the Vicat needle penetration. In accordance with EN 196-3 [7], the time of initial setting was defined as the time at which the penetration depth of the needle was 34 mm, and the time of final setting was defined as the time at which the penetration depth of the needle was 0.5 mm. Table 4 indicates the times of initial and final setting for all tested samples.

4.2 Multi-purpose incremental loading device

The results of the penetrometer experiments conducted on the MIL-device are shown in Fig. 3. When the results of the two unaccelerated samples CEM A and CEM B are compared, it is obvious that the force required to drive the ball deeper into the sample increases at a relatively low rate at the beginning of the measurement. After a certain time, this force starts to increase significantly faster. A comparable development of the force can be observed for the samples CEM A_CN, CEM B_CN, and CEM B_TEA. Different behavior is shown by the sample CEM A_TEA. Here, the required force increases sharply right from the beginning of the measurement, but the rate at which the force increases changes only moderately during the measurement. The transition of the initial rate of penetration resistance to the increased rate of penetration resistance of the samples CEM A and CEM A_TEA occurs at approximately 70 min of

Table 4 Initial and final setting according to EN 196-3

Sample	Initial setting (min)	Final setting (min)
CEM A	160	245
CEM A_CN	124	200
CEM A_TEA	213	312
CEM B	142	245
CEM B_CN	150	221
CEM B_TEA	213	375

hydration. For sample CEM A_CN, this transition occurs at 40 min of hydration.

4.3 Isothermal heat flow calorimetry

In Fig. 4, the development of the heat flow as well as the cumulative heat of hydration, measured over the first 6 h of hydration by isothermal heat flow calorimetry, is shown for all tested cement pastes. All samples show a high initial heat flow between 30 and just over 40 mW/g. For CEM A_TEA, the initial heat flow is significantly higher with 40.1 mW/g than for CEM A (31.7 mW/g) and CEM A_CN (30.6 mW/g). For CEM B none of the accelerators leads to such behavior. With 38.8 mW/g the initial heat flow of CEM B_TEA is only moderately higher than that of the reference sample CEM B (36.1 mW/g). After the short period of the initial heat flow, all samples achieve their minimum heat flow between 75 and 90 min of hydration (induction period). The results show that the minimum heat flow reached by the $\text{Ca}(\text{NO}_3)_2$ -accelerated samples is higher than that of the corresponding reference samples and TEA-accelerated samples. To be able to compare the onset of the acceleration period among the different samples, the onset was defined based on [36] as the intersection of a linear fit to the heat flow between 2 and 4 mW/g and the minimal heat flow of each sample. The onset of the acceleration period, as well as the initial and final setting of each sample, are highlighted in Fig. 4.

4.4 Ultrasonic P-wave velocity measurement

The ultrasonic P-wave velocity development and its first derivative during the first 6 h of hydration are shown in Fig. 5. The P-wave velocity starts to increase

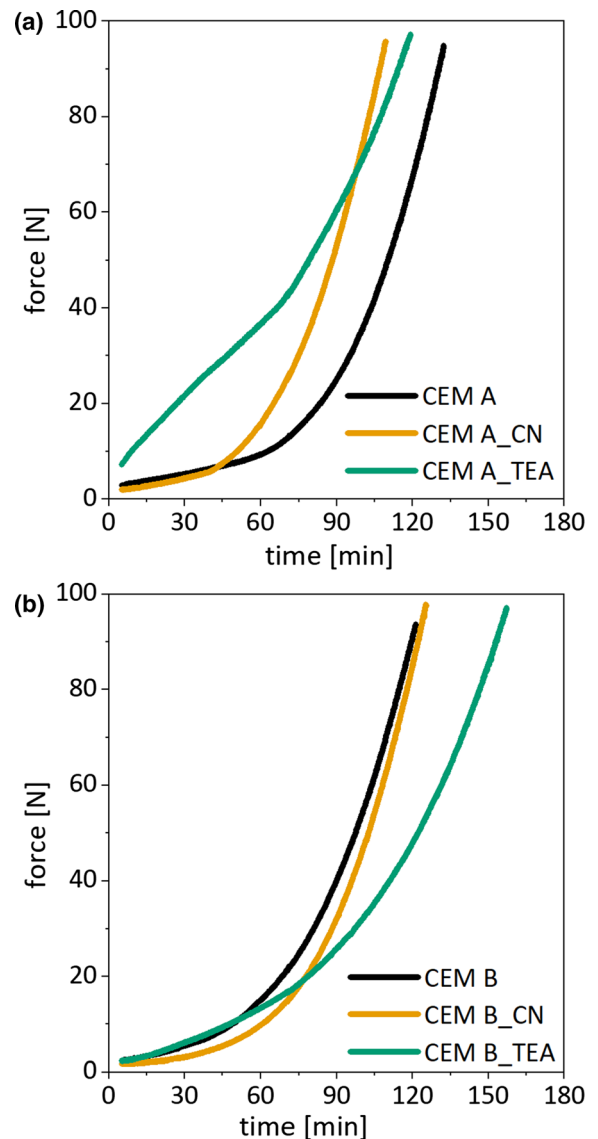


Fig. 3 Results of the penetrometer tests conducted on the MIL-device. **a** Results of CEM A, **b** Results of CEM B

right after the start of each measurement. Until the initial setting time (according to the Vicat needle test) is reached, v_p increases from around 170 m/s to at least 1230 m/s. For each sample, the development of the P-wave velocity starts with a steep increase, which temporarily flattens at approximately the time of the initial setting. The increase in the P-wave velocity becomes steeper again at the final setting time, or for some samples shortly afterwards, and then maintains its slope until the end of the measurement. After 77 min for CEM A_TEA and after 40 min for

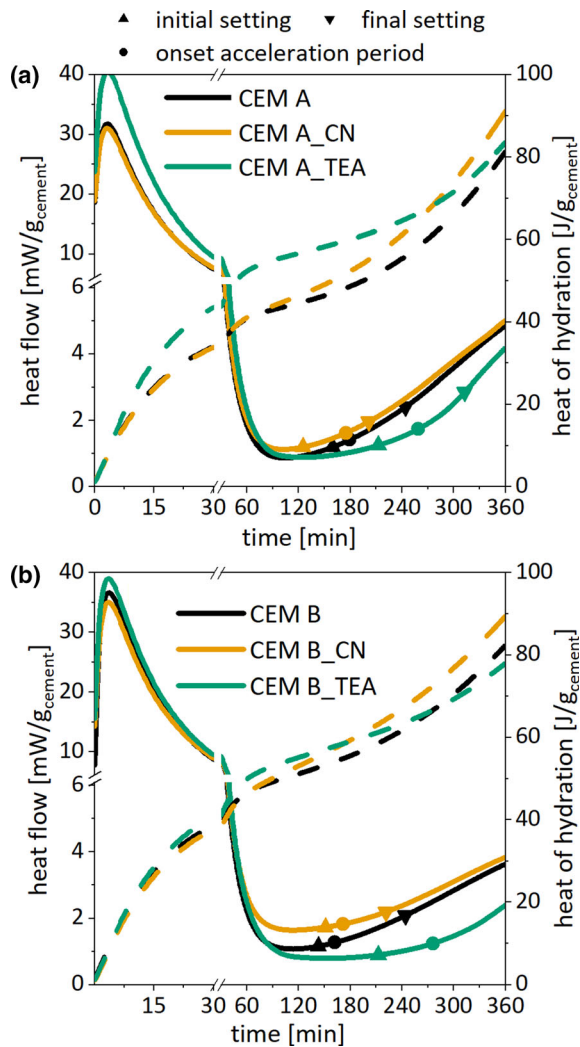


Fig. 4 Heat flow development (straight lines) and cumulative heat (dashed lines) of hydration of all tested samples. **a** Heat flow and cumulative heat of CEM A, **b** heat flow and cumulative heat of CEM B

CEM B_TEA, the rate of the ultrasonic P-wave velocity development temporarily falls behind that of the corresponding reference sample. Thus, at any given point later than 90 min of hydration, CEM A_TEA and CEM B_TEA show a lower ultrasonic P-wave velocity than their corresponding reference samples.

4.5 In-situ XRD

The quantification of crystalline phases based on the minimization of deviations between an observed and a

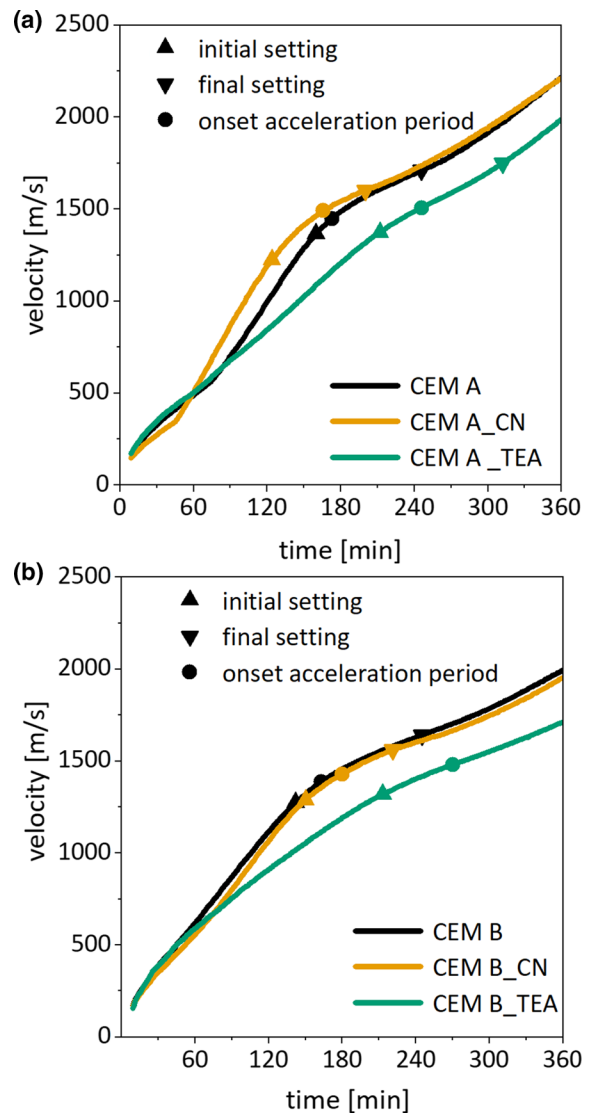


Fig. 5 Evolution of the ultrasonic P-wave velocity. Filled triangle indicates the initial setting time (Vicat), Filled down triangle indicates the final setting time (Vicat), Filled circle indicates the onset of the acceleration period. **a** Evolution of the ultrasonic P-wave velocity of CEM A, **b** evolution of the ultrasonic P-wave velocity of CEM B

calculated X-ray diffraction pattern, as performed during a Rietveld refinement, requires the following to generate reliable results: finely ground powders with a random orientation of crystals, knowledge of all mineral phases contained in a given sample as well as their crystal structures, an internal or external standard to account for the amorphous content if present, and a precise fit of the background [11, 37]. Even though some researchers have succeeded in



quantifying the development of hydration products in hydrating cement pastes by applying an external standard method to in-situ XRD data [11, 12, 14], it remains a sophisticated method. The crystalline phases contained within the sample, the amorphous content, and consequently the measured background signal are continuously changing during the initial stages of hydration. Additionally, the hydration products are not necessarily randomly oriented, as they might grow with a preferred orientation. The authors of the present study therefore decided to limit the analysis of the in-situ XRD results to the comparison of reflex intensity development, which does not offer a quantitative analysis but still provides a qualitative understanding of the hydration process. The development of the intensities for the alite reflex 205, the portlandite reflex 001, the ettringite reflex 010, the tricalcium aluminate reflex 044, and the brownmillerite reflex 411 are shown in Figs. 6 and 7 for all tested samples. The times of initial and final setting are highlighted for every measurement.

The precision of a single in-situ XRD measurement, indicating the variability between different measurements on the same analyte, was estimated by us based on the observation of Jansen et al. [12]. According to this, a dissolution of alite in the in-situ XRD measurements only occurs at the end of the induction period. Consequently, the alite intensity during the first 60 min of hydration should be constant, and the variation of the alite intensity observed in the experiment can be used to calculate the coefficient of variation. The calculated coefficients of variation were in the range between 1 and 2% for each sample. Therefore, intensity variations larger than 2% can be considered significant.

Figures 6 and 7 show that for the samples containing TEA, no portlandite can be detected by XRD, while the reflex intensity of alite stays constant during the entire time of measurement. Figure 6 further shows that the intensity of ettringite rises quickly to a high level of 1125 cps at 10 min of hydration in sample CEM A_TEA, while the intensity of brownmillerite is reduced, by approximately one third as compared to the brownmillerite intensity measured in samples CEM A and CEM A_CN. In contrast, the reference sample CEM A shows an ettringite intensity of 465 cps at 10 min of hydration and 800 cps after 360 min of hydration, while the intensity of brownmillerite stays approximately constant. The time of the

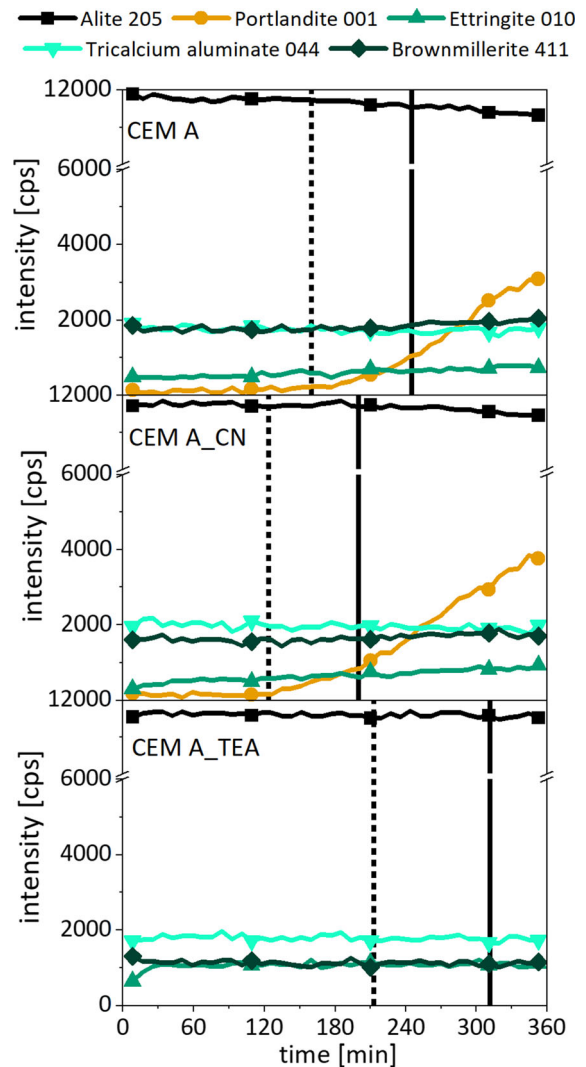


Fig. 6 Reflex intensity development of the alite 205, portlandite 001, ettringite 010, tricalcium aluminate 044, and brownmillerite 411 reflexes in CEM A measured by in-situ XRD. The dotted vertical lines indicate the time of initial setting (Vicat), and the solid vertical lines indicate the time of final setting (Vicat)

onset of the alite reflex decrease as well as the portlandite reflex increase coincide with the initial setting for the samples that do not contain TEA (Figs. 6, 7).

5 Discussion

The discussion of the presented results is separated into two sections. In the first section, the influence of

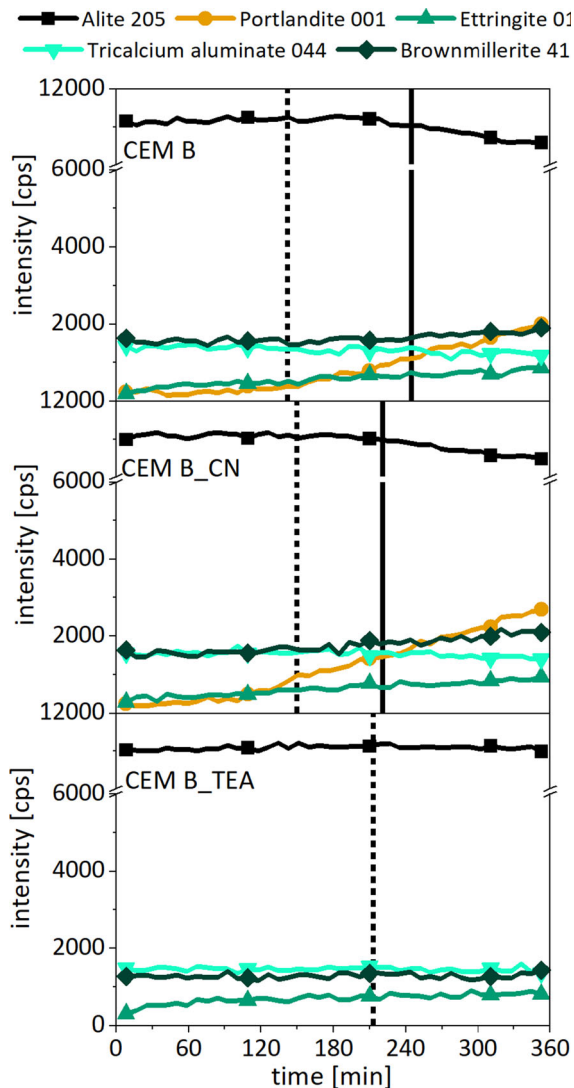


Fig. 7 Reflex intensity development of the alite 205, portlandite 001, ettringite 010, tricalcium aluminate 044, and brownmillerite 411 reflexes in CEM A measured by in-situ XRD. The dotted vertical lines indicate the time of initial setting (Vicat), and the solid vertical lines indicate the time of final setting (Vicat)

the two accelerating admixtures $\text{Ca}(\text{NO}_3)_2$ and TEA on the formation of hydration products and the dissolution of clinker phases during the early stages of cement hydration will be discussed based on the presented results of isothermal calorimetry (Fig. 4) and in-situ XRD (Figs. 6, 7) starting with the initial dissolution. In the second section, the focus will be laid on the correlation between the hydration product formation and the workability reduction of the

material, which was analyzed using Vicat needle penetration test (Fig. 2), MIL-device penetration test (Fig. 3), and ultrasonic P-wave velocity measurement (Fig. 5). The close correlation between the hydration product formation and the workability reduction of the material is highlighted in Fig. 8, which exemplifies all measurement results for CEM A.

The initial heat flow of CEM A is not significantly influenced by the addition of 2.0 wt% $\text{Ca}(\text{NO}_3)_2$ as shown in Fig. 4.

The addition of 0.1 wt% TEA to CEM A leads to an enhanced initial heat flow (Fig. 4), and in-situ XRD (Fig. 6) reveals several reasons for this as the initial dissolution of clinker phases, especially brownmillerite, was intensified. Such an amplified dissolution consequently leads to an enforced precipitation, which is especially clearly visible for ettringite.

During the induction period, increased heat flow was observed for CEM A_CN (Fig. 4). In-situ XRD (Fig. 6) reveals a significant increase in portlandite reflex intensity starting at 120 min and thus 60 min earlier than in the reference sample, it is assumed that $\text{Ca}(\text{NO}_3)_2$ shortens the induction period by enhancing the hydration of alite and the formation of portlandite as well as C-S-H phases.

TEA significantly extended the duration of the induction period as seen in calorimetry. Accordingly, no significant decrease in alite reflex intensity was observed by in-situ XRD (Fig. 6). There are at least two effects of TEA that delay and at high dosages even suppress the main hydration of alite. On the one hand, TEA itself seems to significantly delay (or suppress) the main hydration of alite. Ramachandran [32] proposes the hypothesis that the retarded alite hydration originates from the formation of a Ca^{2+} -TEA complex that becomes strongly adsorbed into the alite surface. According to Ramachandran, this complex forms a layer of reduced permeability on the alite surface and thus increases the induction period. The formation of the Ca^{2+} -TEA complex was further investigated and confirmed by Yang-Rong et al. [31], but there are still no conclusive results demonstrating that the Ca^{2+} -TEA complex is responsible for the retardation of alite hydration, and the mechanism leading to the retardation of alite hydration will need further investigation. On the other hand, TEA can enhance the initial dissolution of the aluminate-bearing clinker phases (especially of brownmillerite), which is shown in the current study as well as in

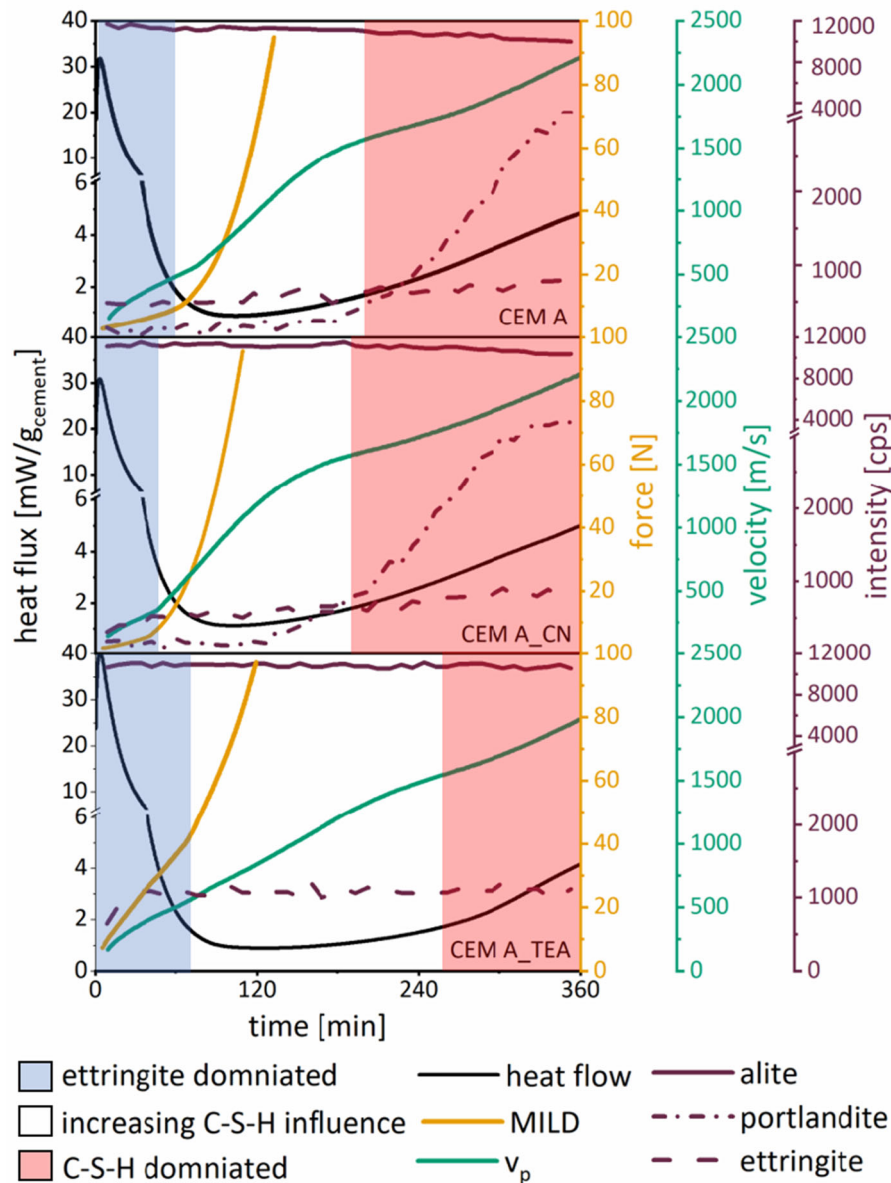


Fig. 8 Summarized results of isothermal calorimetry, MIL-device penetration test, ultrasonic P-wave velocity measurement and in-situ XRD for CEM A

literature [38]. This facilitated initial dissolution can lead to a higher aluminum concentration in the pore solution, which in turn can disturb the onset of the alite main hydration [39–43]. The mechanism behind this is still under discussion [20, 44].

Concerning the hydration of CEM B, the same tendencies as for CEM A can be observed. However, the effects of the two admixtures on CEM B are significantly weaker than for CEM A. $\text{Ca}(\text{NO}_3)_2$

enhances the heat flow of CEM B during the induction period but does not seem to have any further significant effect on the early hydration of CEM B. Also CEM B_TEA shows only a slightly elevated initial heat flow and the enhanced brownmillerite dissolution and amplified intensity of the 010 ettringite reflex already described for CEM A_TEA are also less significant in the case of CEM B_TEA (Fig. 7). It was found that both cements show comparable contents of

C_3A and C_4AF as determined by the quantitative analysis of XRD data by Rietveld refinement (Table 2). CEM B however, shows lower intensities of C_3A and C_4AF in the in-situ XRD measurements (Fig. 7) as compared to sample CEM A (Fig. 6), which might be interpreted as a semiquantitative indication of lower C_3A and C_4AF contents in CEM B. Based on this observation, it might be suspected that the initial reactivity of C_3A and C_4AF is higher in CEM B as compared to CEM A. Thus, it is proposed that as the reactivity of the aluminate phases in CEM B is already high in the absence of TEA, the capacity of TEA to accelerate the aluminate phases in CEM B further is comparably low. Aggoun et al. [45], who analyzed the efficiency of $Ca(NO_3)_2$ to act as an accelerator, described a correlation between the accelerating efficiency of $Ca(NO_3)_2$ and the aluminate phase content of the analyzed cements. Aggoun et al. [45] described that in a high C_3A containing cement $Ca(NO_3)_2$ had almost no effect on the setting time, while in a low C_3A containing cement $Ca(NO_3)_2$ significantly reduces the setting time. Thus, the increased initial reactivity of C_3A and C_4AF in CEM B might be responsible for the reduced efficiency of $Ca(NO_3)_2$ in decreasing the workability and reducing the initial and final setting time of sample CEM B_CN.

Based on the results discussed above, it is suggested that the accelerating effect of $Ca(NO_3)_2$ on the hydration of the analyzed cement pastes might be summarized as enhancing the hydration of alite and the formation of C–S–H. The influence of TEA might be summarized as enhancing the dissolution of C_3A and C_4AF and consequently contributing to ettringite formation while delaying the hydration of alite and the formation of C–S–H phases.

In all samples, an immediate increase in penetration resistance (Fig. 3) and the ultrasonic P-wave velocity (Fig. 5) have been found. This indicates that workability started to decrease right after the addition of water or accelerator solution, respectively. It is well known [46–48] that consumption of water causes an increase in the P-wave velocity through the formation of hydration products, the corresponding transformation of the cement paste from a slurry to a porous solid, and the preferred propagation of compressional waves through the interconnected solids. Thus, the immediate increase of the ultrasonic P-wave velocity might be ascribed to an initial formation of hydration products. As Fig. 8 shows that the ettringite reflex intensity

measured by in-situ XRD starts to increase simultaneously to the ultrasonic P-wave velocity at the beginning of hydration, it is concluded that the formation of ettringite causes the initial loss of workability. The observation further supports this conclusion that the described early loss of workability was most significant for sample CEM A_TEA which undergoes, as discussed above, a significantly enforced ettringite precipitation during the initial period of cement hydration. In Fig. 8, the initial period, in which ettringite is predominantly responsible for the loss of workability, and during which TEA is thus more effective in reducing the workability than $Ca(NO_3)_2$, is highlighted in light blue.

After one hour of hydration, the heat flow of all samples reached a local minimum, the induction period, which is widely regarded as a phase of low chemical activity and slow formation of C–S–H nuclei [16–19] as well as slow ettringite precipitation [11, 20]. Figure 8 shows that during the induction period, the penetration resistance measured by MIL-device and the ultrasonic P-wave velocity increased. This indicates a continued decrease of the material workability, of which the rate is highest for the $Ca(NO_3)_2$ containing samples and lowest for the TEA containing samples. The rapid workability reduction in sample CEM A_CN, as well as sample CEM B_CN (Fig. 3), might be ascribed to the enhancing effect of $Ca(NO_3)_2$ on the hydration of alite and the formation of C–S–H. As the retarding effect of TEA on alite hydration at dosages ≥ 0.1 wt% is well known in literature [28, 30, 32, 33, 49, 50] and was also observed in the present study, the comparatively slow rate of workability reduction in the TEA-containing sample after 60 min of hydration might be a consequence of the delayed C–S–H formation. These observations regarding the influence of $Ca(NO_3)_2$ and TEA on the rate of workability reduction during the induction period indicate that while ettringite has the primary influence on the material workability during the initial period, the formation of C–S–H has the primary influence on workability during the induction period.

Figure 8, in which the acceleration period is highlighted in light red, shows that the increase in the portlandite 001 reflex intensity occurs simultaneously with the increase in heat flow at the beginning of the acceleration period, with the decline in the alite 205 reflex intensity following shortly after. A decline in alite reflex intensity could not be observed for CEM

A_{TEA} during the 6 h of measuring time because of the delayed onset of fast alite hydration already described above. According to [10], the observed decrease of alite and increase in portlandite reflex intensity is connected to the progressing dissolution of alite and the formation of C–S–H phases. It can thus be concluded that the onset of the acceleration period coincides with the beginning of rapid alite hydration, which was previously described by [10, 51] and that the workability reduction during the acceleration period, indicated by a continued increase of ultrasonic P-wave velocity, is dominated by the rapid formation of C–S–H. According to the Vicat needle penetration test, the onset of the acceleration period was located between the initial and final setting time for all tested samples (Fig. 4). This suggests that the setting of the analyzed cement pastes, according to the Vicat needle penetration test, depends mainly on the hydration of alite and the formation of C–S–H phases.

As the hydration of alite and the formation of C–S–H phases are enhanced in the presence of Ca(NO₃)₂, the initial and final setting, the onset of the acceleration period and thus the period in which the fast formation of C–S–H phases mainly dominates the workability were found to occur earlier in Ca(NO₃)₂ accelerated samples. For the TEA accelerated samples, the onset of the acceleration period and the workability reduction based on the fast formation of C–S–H phases were delayed.

6 Conclusions

The presented results are obtained by the analysis of the hydration mechanisms of two CEM I 52.5 R [35] produced by two different manufacturers in the presence of the two accelerating admixtures Ca(NO₃)₂ at a dosage of 2.0 wt% and TEA at a dosage of 0.1 wt% in respect to cement.

Regarding the influence of the two accelerating admixtures on the early hydration mechanisms of the tested cements, it was found that Ca(NO₃)₂ had no significant influence on the initial heat flow but increased the heat flow during the induction period. It seems likely that the addition of Ca(NO₃)₂ enhances the hydration of alite and consequently the formation of C–S–H phases.

At a dosage of 0.1 wt%, TEA significantly increased the initial dissolution of brownmillerite

and the formation of ettringite in CEM A. TEA further extended the duration of the induction period and consequently delayed the onset of the main alite hydration. Two mechanisms that contribute to the delayed onset of alite hydration in the presence of TEA have been discussed.

Results of the ultrasonic P-wave velocity measurements and the conducted penetration tests indicate that in all analyzed samples, workability started to decrease immediately after the addition of water or accelerator solution, respectively. Based on the correlation between the ultrasonic P-wave velocity and penetration tests with the hydration product formation analyzed using isothermal heat flow calorimetry and in-situ XRD, it was suggested that the formation of ettringite is the primary influence on the rate at which the analyzed cement pastes changed their workability during the initial period of hydration.

It was further demonstrated that the formation of C–S–H phases starts to override the effect of ettringite formation on the workability reduction during the induction period and that the formation of C–S–H phases dominates the rate of workability reduction during the acceleration period.

The extent to which the workability of a given cement paste changed significantly depended on the accelerator and its interaction with the cement. Ca(NO₃)₂ was found to have significant effects on the workability of the analyzed cement pastes only after the initial period. Ca(NO₃)₂ enhanced the hydration of alite, the rate of workability loss during the induction period, and advanced the onset of the acceleration period as well as the initial and final setting time. TEA enhanced the precipitation of ettringite and thereby significantly reduced the workability within the first 60 min of cement hydration. By retarding the onset of fast alite hydration, TEA, however, prolonged the induction period, increased the initial and final setting time, and delayed the onset of workability reduction based on the fast formation of C–S–H phases.

It has been demonstrated that ultrasonic P-wave velocity measurements as well as penetration tests can be effectively used to continuously monitor the changing workability of accelerated cement pastes. In contrast to the Vicat needle penetration test, which was shown to depend on the formation of C–S–H phases mainly, both methods were demonstrated to be sensitive towards the early workability change due to



the initial formation of ettringite. As it seems likely that these results will be transferable to mortars and concretes, both methods might be applicable in the development of 3D-printable cement-based materials for which focus has to be laid on a continuous monitoring of the workability in order to estimate printability and buildability at any given time of the hydration.

Acknowledgements The authors acknowledge the German Federal Ministry of Education and Research for funding this work in the scope of the project BauProAddi (FKZ:03XP0122A). Furthermore, the authors would like to thank Carl Sievers for his contribution to this publication.

Funding Open Access funding enabled and organized by Projekt DEAL.. This work was funded by the German Federal Ministry of Education and Research in the scope of the project BauProAddi (FKZ: 03XP0122A).

Data availability Data can be provided upon request.

Code availability Not applicable.

Declarations

Conflict of interest The authors declare that they have no conflict of interest.

Open Access This article is licensed under a Creative Commons Attribution 4.0 International License, which permits use, sharing, adaptation, distribution and reproduction in any medium or format, as long as you give appropriate credit to the original author(s) and the source, provide a link to the Creative Commons licence, and indicate if changes were made. The images or other third party material in this article are included in the article's Creative Commons licence, unless indicated otherwise in a credit line to the material. If material is not included in the article's Creative Commons licence and your intended use is not permitted by statutory regulation or exceeds the permitted use, you will need to obtain permission directly from the copyright holder. To view a copy of this licence, visit <http://creativecommons.org/licenses/by/4.0/>.

References

- Labonnote N, Rønquist A, Manum B et al (2016) Additive construction. State-of-the-art, challenges and opportunities. *Autom Constr* 72:347–366. <https://doi.org/10.1016/j.autcon.2016.08.026>
- Pfeiffer S, Stephan D, Dorn T et al. State of the art and perspectives of 3D printing in construction. In: Leopolder F (ed) *Dry mix mortar yearbook—3D special*, München, pp 22–32
- Marchon D, Kawashima S, Bessaies-Bey H et al (2018) Hydration and rheology control of concrete for digital fabrication. Potential admixtures and cement chemistry. *Cem Concr Res* 112:96–110. <https://doi.org/10.1016/j.cemconres.2018.05.014>
- Le TT, Austin SA, Lim S et al (2012) Mix design and fresh properties for high-performance printing concrete. *Mater Struct* 45(8):1221–1232. <https://doi.org/10.1617/s11527-012-9828-z>
- Lim S, Buswell RA, Le TT et al (2012) Developments in construction-scale additive manufacturing processes. *Autom Constr* 21:262–268. <https://doi.org/10.1016/j.autcon.2011.06.010>
- Perrot A, Rangeard D, Pierre A (2016) Structural built-up of cement-based materials used for 3D-printing extrusion techniques. *Mater Struct* 49(4):1213–1220. <https://doi.org/10.1617/s11527-015-0571-0>
- EN 196-3:2016 (2017) Methods of testing cement. Part 3: determination of setting times and soundness
- Bullard JW, Jennings HM, Livingston RA et al (2011) Mechanisms of cement hydration. *Cem Concr Res* 41(12):1208–1223. <https://doi.org/10.1016/j.cemconres.2010.09.011>
- Scrivener KL, Nonat A (2011) Hydration of cementitious materials, present and future. *Cem Concr Res* 41(7):651–665. <https://doi.org/10.1016/j.cemconres.2011.03.026>
- Jansen D, Goetz-Neunhoeffler F, Lothenbach B et al (2012) The early hydration of ordinary portland cement (OPC): an approach comparing measured heat flow with calculated heat flow from QXRD. *Cem Concr Res* 42(1):134–138. <https://doi.org/10.1016/j.cemconres.2011.09.001>
- Hesse C, Goetz-Neunhoeffler F, Neubauer J (2011) A new approach in quantitative in-situ XRD of cement pastes: correlation of heat flow curves with early hydration reactions. *Cem Concr Res* 41(1):123–128. <https://doi.org/10.1016/j.cemconres.2010.09.014>
- Jansen D, Goetz-Neunhoeffler F, Stabler C et al (2011) A remastered external standard method applied to the quantification of early OPC hydration. *Cem Concr Res* 41(6):602–608. <https://doi.org/10.1016/j.cemconres.2011.03.004>
- Pott U, Ehm C, Jakob C et al. Investigation of the early cement hydration with a new penetration test, rheometry and in-situ XRD. In: 2nd International RILEM conference, rheology and processing of construction materials (Rheo-Con2), Dresden, Germany, 8th–11th September 2019, pp 246–255
- Jakob C, Jansen D, Pott U et al (2019) Comparing phase development and rheological properties of OPC paste within the first hour of hydration. In: 2nd International RILEM conference, rheology and processing of construction materials (Rheo-Con2), Dresden, Germany, 8th–11th September 2019, pp 219–227
- Jakob C, Jansen D, Ukrainczyk N et al (2019) Relating ettringite formation and rheological changes during the initial cement hydration: a comparative study applying XRD analysis, rheological measurements and modeling. *Materials* 12(18):5–6. <https://doi.org/10.3390/ma12182957>
- Damidot D, Nonat A, Barret P (1990) Kinetics of tricalcium silicate hydration in diluted suspensions by microcalorimetric measurements. *J Am Ceram Soc* 73(11):3319–3322. <https://doi.org/10.1111/j.1151-2916.1990.tb06455.x>



17. Juilland P, Gallucci E, Flatt R et al (2010) Dissolution theory applied to the induction period in alite hydration. *Cem Concr Res* 40(6):831–844. <https://doi.org/10.1016/j.cemconres.2010.01.012>
18. Bazzoni A (2014) Study of early hydration mechanisms of cement by means of electron microscopy, Thèse EPFL n°6296. Dissertation, École Polytechnique Fédérale de Lausanne
19. Gallucci E, Mathur P, Scrivener KL (2010) Microstructural development of early age hydration shells around cement grains. *Cem Concr Res* 40(1):4–13. <https://doi.org/10.1016/j.cemconres.2009.09.015>
20. Bergold ST, Goetz-Neunhoeffer F, Neubauer J (2017) Interaction of silicate and aluminate reaction in a synthetic cement system: implications for the process of alite hydration. *Cem Concr Res* 93:32–44. <https://doi.org/10.1016/j.cemconres.2016.12.006>
21. Powers TC (1958) Structure and physical properties of hardened portland cement paste. *J Am Ceram Soc* 41(1):1–6. <https://doi.org/10.1111/j.1151-2916.1958.tb13494.x>
22. Ylmén R, Jäglid U, Steenari B-M et al (2009) Early hydration and setting of Portland cement monitored by IR, SEM and Vicat techniques. *Cem Concr Res* 39(5):433–439. <https://doi.org/10.1016/j.cemconres.2009.01.017>
23. Roussel N, Ovarlez G, Garrault S et al (2012) The origins of thixotropy of fresh cement pastes. *Cem Concr Res* 42(1):148–157. <https://doi.org/10.1016/j.cemconres.2011.09.004>
24. Justnes H, Nygaard EC (1995) Technical calcium nitrate as set accelerator for cement at low temperatures. *Cem Concr Res* 25(8):1766–1774. [https://doi.org/10.1016/0008-8846\(95\)00172-7](https://doi.org/10.1016/0008-8846(95)00172-7)
25. Myrdal R, Sintef (2007) Accelerating admixtures for concrete. State of the art (978-82-536-0989-8): 1–35. Accessed 13 Jun 2018
26. Chikh N, Cheikh-Zouaoui M, Aggoun S et al (2007) Effects of calcium nitrate and triisopropanolamine on the setting and strength evolution of Portland cement pastes. *Mater Struct* 41(1):31–36. <https://doi.org/10.1617/s11527-006-9215-8>
27. Dorn T, Hirsch T, Stephan D (2019) Study on the influence of accelerators on the hydration of Portland cement and their applicability in 3D printing. In: Mechtcherine, Viktor, Khayat, Kamal, Secrieru, Egor (eds) *Rheology and processing of construction materials*. RheoCon2 & SCC9. Springer, Basingstoke
28. Ramachandran VS (1972) Influence of triethanolamine on the hydration characteristics of tricalcium silicate. *J Appl Chem Biotechnol* 22(11):1125–1138. <https://doi.org/10.1002/jctb.5020221102>
29. Jachiet M, Azéma N, Le Saoût G et al (2018) Influence of triethanolamine on cement pastes at early age of hydration. *Adv Cem Res* 30(4):159–171. <https://doi.org/10.1680/jadcr.17.00041>
30. Kong X-M (2012) Effect of organic grinding aids on cement properties and the analysis via organic cement chemistry. *J Chin Ceram Soc* 40(1):50–55
31. Yan-Rong Z, Xiang-Ming K, Zi-Chen L et al (2016) Influence of triethanolamine on the hydration product of portlandite in cement paste and the mechanism. *Cem Concr Res* 87:64–76. <https://doi.org/10.1016/j.cemconres.2016.05.009>
32. Ramachandran V (1976) Hydration of cement—role of triethanolamine. *Cem Concr Res* 6(5):623–631. [https://doi.org/10.1016/0008-8846\(76\)90026-0](https://doi.org/10.1016/0008-8846(76)90026-0)
33. Yaphary YL, Yu Z, Lam RH et al (2017) Effect of triethanolamine on cement hydration toward initial setting time. *Constr Build Mater* 141:94–103. <https://doi.org/10.1016/j.conbuildmat.2017.02.072>
34. Ramachandran VS (1973) Action of triethanolamine on the hydration of tricalciumaluminate. *Cem Concr Res* 3:41–54
35. EN 197-1:2011 Cement. Part 1: Composition, specifications and conformity criteria for common cements, 2011
36. von Daake H, Stephan D (2016) Setting of cement with controlled superplasticizer addition monitored by ultrasonic measurements and calorimetry. *Cem Concr Compos* 66:24–37. <https://doi.org/10.1016/j.cemconcomp.2015.11.004>
37. Le Saoût G, Kocaba V, Scrivener K (2011) Application of the Rietveld method to the analysis of anhydrous cement. *Cem Concr Res* 41(2):133–148. <https://doi.org/10.1016/j.cemconres.2010.10.003>
38. Gartner E, Myers D (1993) Influence of tertiary alkanolamines on Portland cement hydration. *J Am Ceram Soc* 76(6):1521–1530. <https://doi.org/10.1111/j.1151-2916.1993.tb03934.x>
39. Nicoleau L, Schreiner E, Nonat A (2014) Ion-specific effects influencing the dissolution of tricalcium silicate. *Cem Concr Res* 59:118–138. <https://doi.org/10.1016/j.cemconres.2014.02.006>
40. Quennoz A, Scrivener KL (2013) Interactions between alite and C3A-gypsum hydrations in model cements. *Cem Concr Res* 44:46–54. <https://doi.org/10.1016/j.cemconres.2012.10.018>
41. Suraneni P, Flatt RJ (2015) Use of micro-reactors to obtain new insights into the factors influencing tricalcium silicate dissolution. *Cem Concr Res* 78:208–215. <https://doi.org/10.1016/j.cemconres.2015.07.011>
42. Odler I, Schüppstuhl J (1981) Early hydration of tricalcium silicate III. Control of the induction period. *Cem Concr Res* 11(5–6):765–774. [https://doi.org/10.1016/0008-8846\(81\)90035-1](https://doi.org/10.1016/0008-8846(81)90035-1)
43. Mota B, Matschei T, Scrivener K (2015) The influence of sodium salts and gypsum on alite hydration. *Cem Concr Res* 75:53–65. <https://doi.org/10.1016/j.cemconres.2015.04.015>
44. Begarin F, Garrault S, Nonat A et al (2011) Hydration of alite containing aluminium. *Adv Appl Ceram* 110(3):127–130. <https://doi.org/10.1179/1743676110Y.0000000007>
45. Aggoun S, Cheikh-Zouaoui M, Chikh N et al (2008) Effect of some admixtures on the setting time and strength evolution of cement pastes at early ages. *Constr Build Mater* 22(2):106–110. <https://doi.org/10.1016/j.conbuildmat.2006.05.043>
46. Sayers CM, Dahlin A (1993) Propagation of ultrasound through hydrating cement pastes at early times. *Adv Cem Based Mater* 1(1):12–21. [https://doi.org/10.1016/1065-7355\(93\)90004-8](https://doi.org/10.1016/1065-7355(93)90004-8)



47. Sayers CM, Grenfell RL (1993) Ultrasonic propagation through hydrating cements. *Ultrasonics* 31(3):147–153. [https://doi.org/10.1016/0041-624X\(93\)90001-G](https://doi.org/10.1016/0041-624X(93)90001-G)
48. Voigt T, Grosse CU, Sun Z et al (2005) Comparison of ultrasonic wave transmission and reflection measurements with P- and S-waves on early age mortar and concrete. *Matériaux et Construction* 38(8):729–738. <https://doi.org/10.1007/BF02479285>
49. Kong X-M, Lu Z-B, Liu H et al (2013) Influence of tri-ethanolamine on the hydration and the strength development of cementitious systems. *Mag Concr Res* 65(18):1101–1109. <https://doi.org/10.1680/macr.13.00015>
50. Xu Z, Li W, Sun J et al (2017) Research on cement hydration and hardening with different alkanolamines. *Constr Build Mater* 141:296–306. <https://doi.org/10.1016/j.conbuildmat.2017.03.010>
51. Thomas JJ, Jennings HM, Chen JJ (2009) Influence of nucleation seeding on the hydration mechanisms of tricalcium silicate and cement. *J Phys Chem C* 113(11):4327–4334. <https://doi.org/10.1021/jp809811w>

Publisher's Note Springer Nature remains neutral with regard to jurisdictional claims in published maps and institutional affiliations.

